

Effect of Axial Stresses of the Core on the Free Vibration Response of a Sandwich Beam with FG Carbon Nanotube Faces and Stiff and Flexible Cores

S. Etehad, M. Botshekanan Dehkordi*

Mechanical Engineering Department, Shahrekord University, Shahrekord, Iran.

Article info

Article history:

Received 15 January 2018

Received in revised form

07 December 2018

Accepted 13 April 2019

Keywords:

Vibration analysis

Sandwich beam

Stiff and flexible core

FG carbon nanotubes

Extended higher order theory

Abstract

In this article, a vibrational behavior of sandwich beams with stiff and flexible cores and face sheets reinforced with carbon nanotubes is investigated. Carbon nanotubes are used as materials with properties varying along the thickness. In order to model the behavior of faces, the Timoshenko beam's theory is employed and also for modeling the behavior of the core, three-dimensional elasticity is used. The axial stresses of the core are considered in this model and therefore it is suitable for modelling two types of stiff and flexible cores. The equations of motion are derived using the variations of energy, and the Navier method is used to solve the equations of motion. Results are presented for different volumes of carbon nanotubes with different distributions along the thickness of the faces. In the case of stiff core, results show that the FG-V distribution has the highest natural frequency and the FG-A distribution has the lowest natural frequency in all cases. For flexible core, the FG-X distribution leads to the highest natural frequency and also the FG-O distribution has the lowest natural frequency. Furthermore, results indicate that an extended high-order sandwich panel theory is a suitable model for analysis of stiff and flexible core sandwich panels. It must be mentioned for the cores made of stiff materials, the normal stress along the length of the core must be considered. It is due to the fact that the obtained results show that ignoring the normal stress along the length of the core leads to the large difference in the natural frequency of the system. In this article, due to the high order displacement field of the core, the flexibility of the core can be seen in the modeling. Additionally, since the term σ_{xx}^c of the core is considered in the strain energy, a stiff core can be modeled. In many works the axial stresses of the core is removed from equations, therefore according to the results of sandwich beam with stiff core, lots of errors will be observed. Therefore, a proposed theory in this research can easily model a sandwich beam with two types of stiff and flexible cores. Since the Timoshenko beam theory is also implemented for modeling faces, different pattern of CNTs can be investigated accurately.

Nomenclature

| | | | |
|-----------------|--------|---------------|--------------|
| σ_{xx} | Stress | τ_{xz} | Shear stress |
| ϵ_{xx} | Strain | γ_{xz} | Shear strain |

*Corresponding author: M. Botshekanan Dehkordi (Assistant Professor)

E-mail address: mbd_dehkordi@yahoo.com

<http://dx.doi.org/10.22084/jrstan.2018.15538.1040>

ISSN: 2588-2597

| | | | |
|-----------------|---|----------|---|
| V_{cn} | Volume fraction of carbon nanotubes | V_m | Volume fraction of the matrix |
| η_1 | Efficiency parameter for scale dependent properties | η_3 | Efficiency parameter for scale dependent properties |
| C_{ij}^c | Stiffness coefficients | k_s | Shear vector |
| σ_{xx}^c | Stress elongation of core | | |

1. Introduction

A sandwich beam is made of two main parts. First, the middle core which is weak and usually bulky. The other one is face sheets on both sides of the core, which are strong and usually thin [1]. Face sheets are usually made of metal sheets or composite sheets, and the core can be made of light polymers, foams, honeycomb structures, or materials with functionally distributed properties. In the recent years plastic foams have been used instead of the lattice core to reduce weight and flexibility. The flexible core makes the beam bendable. The core material should have characteristics such as low density for lowering the weight of the structure and the high vertical Young's modulus to prevent excessive change along the thickness and reduction of flexural stiffness. In most cases, face sheets tolerate the bending loads and the core tolerates the shear loads [2].

The general principles governing sandwich structures are the same despite their high diversity. This simple structure, due to its similar appearance with sandwich, is called a sandwich. A sandwich structure has a much higher resistance compared to its individual components. Frostig et al. [3], in 1990, developed a prominent high-order sandwich panel theory that is a kind of multi-layered theory.

In this theory, face sheets and core are modeled separately. In most researches, due to the flexibility of the core, the in-plane stress for core is discarded due to the low modulus of the flexible core in comparison to the face sheets. But the model presented in this article considered the in-plane stress, therefore it can be applied for the stiff core.

Carbon nanotubes have remarkable mechanical properties [4]. If the carbon nanotubes only contain a pipe of graphite called single-wall nanotubes and if it contains a number of united central tubes a nanotube is called a multi-wall [5]. The use of carbon nanotubes as reinforcement of composites compared to conventional carbon fibers can significantly increase the strength and rigidity of composites [6]. FG carbon nanotubes are functionally graded materials whose mechanical properties change along the thickness. In recent years, this topic has broadly focused studies on bending, vibration, and buckling of structures with functionally graded materials. Wu et al. [7] and Bhangale and Ganesan [8] studied the bending and vibrational properties of sandwich beam with functionally graded face sheets. Shen [9] compared and examined the effect of uniform distribution and functional distribution on the

flexural behavior of carbon nanotube plates. Their result showed functionally graded distributed nanotubes improve the bending behavior of the plates. Shen and Zhu [10] used the high shear deformation theory to study the buckling of nano-carbon reinforced sandwich plates. Their result showed the temperature variation, volume fraction of nanotubes, and the thickness of the coating affect the buckling load of the sandwich plates. Wu et al. [7] studied the vibrational and flexural behavior of sandwich beams with the face sheets of functionally graded carbon nanotubes using the theory of Timoshenko's beam. It was concluded the distributed carbon-nanotubes scaling function had a higher natural frequency and a better bending behavior than uniform distribution. Ansari et al. [11] examined the nonlinear vibrations of composite plates reinforced with carbon nanotubes. The first-order shear deformation theory and Van Kreem's relations were used. Increasing the volume of carbon nanotubes, growth in the flexural hardness of the plate and therefore increase in the natural frequency were observed. Furthermore, it was revealed that the distribution of nanotubes has a significant effect on the vibration behavior of the plates. Ke et al. [12] studied the effect of the volume fraction of carbon nanotubes on nonlinear free vibrations. Their results showed that by increasing the volume fraction of carbon, the natural frequency increases. Frostig [13] explored the behavior of sandwich beams and flexible layered structures. In his studies, the metallic, composite, and foam-made cores and calculated the governing equations for the behavior of these structures were analyzed. In this research, the vibrational behavior of a stiff and flexible core sandwich beam and reinforced composite face sheets with FG carbon nanotubes are investigated. For modeling the face sheets, Timoshenko's theory and also for modeling the behavior of the core, the three-dimensional elasticity, taking into account in-plane stresses, are employed. In order to solve the equations of motion, the Navier method is used. The effect of different volumes of carbon nanotubes, different distribution of nanotubes and different thicknesses of the face sheets on the natural frequency of the system is investigated for two types of stiff and flexible cores.

2. Derivation Equations of Motion

A sandwich beam is composed of a thin face sheet in the top and bottom, as well as a core in the middle of the beam, and the cores and face sheets are stuck to-

gether. In this paper, the core is considered to be stiff and flexible. The upper and lower face sheets are reinforced by carbon nanotubes. The length of the beam is L and the width of the beam is b and the thickness of each layer is h , as shown in Fig. 1, and also the center of coordinates for the layers and core are each in the middle of their thickness.

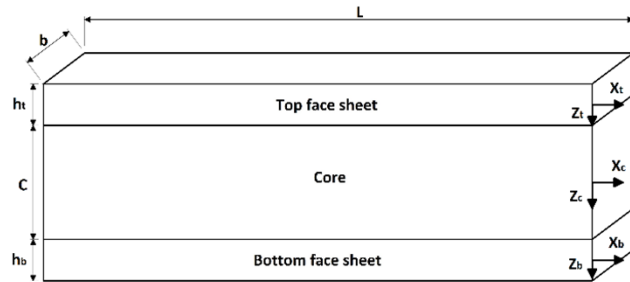


Fig. 1. Geometry and sandwich dimension.

3. Composite Properties

In this research, the face sheets are made of composite reinforced with carbon nanotubes. Therefore, it is necessary to express the mechanical properties of these materials. Hooke's law for mixtures is as follows [14]:

$$\sigma_{xx} = C_{11}^* \epsilon_{xx} \quad (1)$$

$$\tau_{xz} = C_{55}^* \gamma_{xz} \quad (2)$$

$$C_{11}^* = C_{11} m^4 + 2(C_{12} + C_{66}) m^2 n^2 + C_{22} n^4 \quad (3)$$

$$C_{55}^* = C_{55} m^2 + C_{44} n^2 \quad (4)$$

where

$$m = \cos \theta \quad (5)$$

$$n = \sin \theta \quad (6)$$

Angle of the carbon nanotubes with the horizontal axis is θ . As the nanotubes are placed horizontally in the procedure of this study, $\theta = 0$ and relations (3) and (4) are written as follows [14]:

$$C_{11}^* = C_{11} = E_{11} \quad (7)$$

$$C_{55}^* = C_{55} = G_{13} = G_{12} \quad (8)$$

According to the mixing rule for mechanical properties, the modulus of elasticity and shear modulus are written as follows [15]:

$$E_{11} = \eta_1 V_{cn} E_{11}^{cn} + V_m E_m \quad (9)$$

$$\frac{\eta_3}{G_{12}} = \frac{V_{cn}}{G_{12}^{cn}} + \frac{V_m}{G_m} \quad (10)$$

where V_{cn} is the volume fraction of carbon nanotubes, V_m is the volume fraction of the matrix, E_{11}^{cn} is modulus of elasticity of carbon nanotubes, E_m is the matrix

elastic modulus, G_{12}^{cn} is the shear modulus of the carbon nanotubes, G_m is the shear modulus of matrix and η_1 and η_3 are the efficiency parameters for scale dependent properties. Face sheets are considered in the form of a functionally graded carbon nanotube, UD, FG-O, FG-X, FG-V, FG- Λ , and their distribution pattern is shown in Fig. 2. The volume fraction of the carbon nanotubes is a function of the thickness of the face sheets, which is expressed in Table 1 in terms of volume fraction and thickness. In Table 1, V_{cn}^* is a special volume fraction.

Table 1

The ratio of the volume fraction of carbon nanotubes and the thickness.

| Distribution pattern of nano tubes | Volume fraction for top face sheet (V_{cn}) | Volume fraction for bottom face sheet (V_{cn}) |
|------------------------------------|---|--|
| UD | V_{cn}^* | V_{cn}^* |
| FG-O | $2V_{cn}^* \left(1 - 2\frac{ z }{h_t}\right)$ | $2V_{cn}^* \left(1 - 2\frac{ z }{h_b}\right)$ |
| FG-X | $4V_{cn}^* \left(\frac{ z }{h_t}\right)$ | $4V_{cn}^* \left(\frac{ z }{h_b}\right)$ |
| FG-V | $2V_{cn}^* \left(0.5 - \frac{z}{h_t}\right)$ | $2V_{cn}^* \left(0.5 + \frac{z}{h_b}\right)$ |
| FG- Λ | $2V_{cn}^* \left(0.5 + \frac{z}{h_t}\right)$ | $2V_{cn}^* \left(0.5 - \frac{z}{h_b}\right)$ |

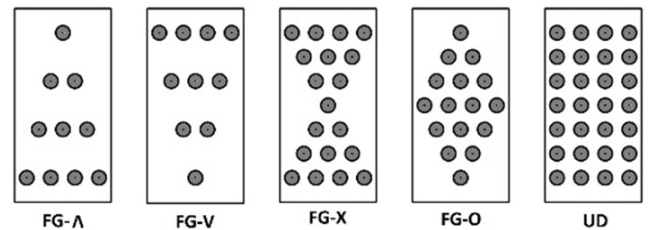


Fig. 2. Distribution pattern of carbon nanotubes.

According to the mixture rules of composite materials, the density of face sheets is as follows [16]:

$$\rho = V_{cn} \rho^{cn} + V_m \rho^m \quad (11)$$

where ρ^{cn} is the density of the carbon nanotubes and ρ^m is the density of the matrix.

4. Displacement

In this paper, the high-order theory of sandwiches is developed. In order to model the face sheets, the Timoshenko's beam theory is employed. Therefore, the displacement field for the face sheets is explained as follows [13]:

$$u^i(x, z, t) = u_O^i(x, t) + z_i \phi^i(x, t) \quad (i = t, b) \quad (12)$$

$$w^i(x, z, t) = w_O^i(x, t) \quad (i = t, b) \quad (13)$$

Strain relations for face sheets are expressed as follows [13]:

$$\epsilon_{xx}^i(x, z, t) = u_{,x}^i(x, z, t) = u_{0,x}^i(x, t) + z\phi_{,x}^i(x, t) \quad (14)$$

$$\begin{aligned} \gamma_{xz}^i(x, z, t) &= u_{,x}^i(x, z, t) + w_{,x}^i(x, z, t) \\ &= \phi^i(x, t) + w_{0,x}^i(x, t) \end{aligned} \quad (15)$$

The displacement field for the core is explained as follows [13]:

$$u^c(x, z, t) = u_0^c(x, t) + u_1^c(x, t)z_c + u_2^c(x, t)z_c^+ + u_3^c(x, t)z_c^3 \quad (16)$$

$$w^c(x, z, t) = w_0^c(x, t) + w_1^c(x, t)z_c + w_2^c(x, t)z_c^2 \quad (17)$$

Due to the continuity of the displacement between the cores and the face sheets, the compatibility relationships are expressed as follows [3]:

$$w^c\left(x, -\frac{c}{2}, t\right) = w^t(x, t) \quad (18)$$

$$u^c\left(x, -\frac{c}{2}, t\right) = u_0^t(x, t) + \frac{h_t}{2}\phi^t(x, t) \quad (19)$$

$$w^c\left(x, \frac{c}{2}, t\right) = w^b(x, t) \quad (20)$$

$$u^c\left(x, \frac{c}{2}, t\right) = u_0^b(x, t) - \frac{h_b}{2}\phi^b(x, t) \quad (21)$$

Employing the compatibility relationships and also applying a series of mathematical manipulations, the core displacement can be defined as follows [3]:

$$\begin{aligned} u^c(x, z, t) &= u_0^c(x, t) + u_1^c(x, t)z_c + \left[\frac{2}{c^2}\left(u_0^t(x, t) + \right. \right. \\ & \left. \left. u_0^b(x, t) - 2u_0^c(x, t) + \frac{h_t}{2}\phi^t(x, t) - \frac{h_b}{2}\phi^b(x, t)\right)\right]z_c^2 + \\ & \left[\frac{4}{c^3}\left(-u_0^t(x, t) - \frac{h_t}{2}\phi^t(x, t) + u_0^b(x, t) \right. \right. \\ & \left. \left. - \frac{h_b}{2}\phi^b(x, t) - c\phi_0^c(x, t)\right)\right]z_c^3 \end{aligned} \quad (22)$$

$$\begin{aligned} w^c(x, z, t) &= w_0^c(x, t) + \frac{1}{c}[w_0^b(x, t) - w_0^t(x, t)]z_c \\ &+ \frac{2}{c^2}[w_0^t(x, t) + w_0^b(x, t) - 2w_0^c(x, t)]z_c^2 \end{aligned} \quad (23)$$

Due to the core displacement field, a flexible core can be modeled. Strain relations for the core are ob-

tained based on linear strains as follows [13]:

$$\epsilon_{xx}^c(x, z, t) = u_{,x}^c(x, z, t) \quad (24)$$

$$\gamma_{xz}^c(x, z, t) = u_{,z}^c(x, z, t) + w_{,x}^c(x, z, t) \quad (25)$$

$$\epsilon_{zz}^c(x, z, t) = w_{,z}^c(x, z, t) \quad (26)$$

The stress and strain relations are based on linear elastic behavior as follows [7]:

$$\begin{bmatrix} \sigma_{xx}^c \\ \sigma_{zz}^c \\ \tau_{xz}^c \end{bmatrix} = \begin{bmatrix} C_{11}^c & C_{13}^c & 0 \\ C_{13}^c & C_{33}^c & 0 \\ 0 & 0 & C_{55}^c \end{bmatrix} \begin{bmatrix} \epsilon_{xx}^c \\ \epsilon_{zz}^c \\ \gamma_{xz}^c \end{bmatrix} \quad (27)$$

where C_{ij}^c ($i, j = 1, 3, 5$) are the stiffness coefficients for orthotropic materials. Equations of motion are obtained based on the Hamilton principle in the following form [7]:

$$\int_{t_1}^{t_2} [\partial T - \partial U] dt = 0 \quad (28)$$

5. Calculation of Strain Energy

The first variation of the strain energy is calculated as follows [7]:

$$\begin{aligned} \delta U &= \int \int \int_{v_{top}} \sigma_{xx} \delta \epsilon_{xx} dv + \int \int \int_{v_{top}} k_s \tau_{xz} \delta \gamma_{xz} dv \\ &+ \int \int \int_{v_{bot}} \sigma_{xx} \delta \epsilon_{xx} dv + \int \int \int_{v_{bot}} k_s \tau_{xz} \delta \gamma_{xz} dv \\ &+ \int \int \int_{v_{core}} \sigma_{xx} \delta \epsilon_{xx} dv + \int \int \int_{v_{core}} \sigma_{zz} \delta \epsilon_{zz} dv \\ &+ \int \int \int_{v_{core}} \tau_{xz} \delta \gamma_{xz} dv \end{aligned} \quad (29)$$

In many works the σ_{xx}^c is removed from equations, therefore according to the results in sandwich beam with stiff core if the σ_{xx}^c is removed from equations, a lot of error in results will be created. Since the stiff core is used in this paper, the σ_{xx}^c in the formula (29) must be considered.

6. Calculation of Kinetic Energy

$$\begin{aligned} \delta T &= - \int_{v_t} \rho^t (\ddot{u}_0^t \delta u_0^t + \ddot{w}_0^t \delta w_0^t) dv \\ &- \int_{v_b} \rho^b (\ddot{u}_0^b \delta u_0^b + \ddot{w}_0^b \delta w_0^b) dv \\ &- \int_{v_c} \rho_c \ddot{u}_c \delta u_c dv - \int_{v_c} \rho_c \ddot{w}_c \delta w_c dv \end{aligned} \quad (30)$$

In relation (30), the acceleration of the core and face sheets are expressed as follows [13]:

$$\ddot{u}^i = \ddot{u}_0^i + z\ddot{\phi}^i \quad (i = t, b) \quad (31)$$

$$\ddot{w}^i = \ddot{w}_0^i \quad (i = t, b) \quad (32)$$

$$\begin{aligned} \ddot{u}_c = \ddot{u}_0^c + \ddot{\phi}_1^c z_c + \left[\frac{2}{c^2} \left(\ddot{u}_0^t + \ddot{u}_0^b - 2\ddot{u}_0^c \right. \right. \\ \left. \left. + \frac{h_t}{2} \ddot{\phi}^t - \frac{h_b}{2} \ddot{\phi}^b \right) \right] z_c^2 + \left[\frac{4}{c^3} \left(-\ddot{u}_0^t \right. \right. \\ \left. \left. - \frac{h_t}{2} \ddot{\phi}^t + \ddot{u}_0^b - \frac{h_b}{2} \ddot{\phi}^b - c\ddot{\phi}_0^c \right) \right] z_c^3 \end{aligned} \quad (33)$$

$$\ddot{w}_c = \ddot{w}_0^c + \frac{1}{c} [\ddot{w}_0^b - \ddot{w}_0^t] z_c + \frac{2}{c^2} [\ddot{w}_0^t + \ddot{w}_0^b - 2\ddot{w}_0^c] z_c^2 \quad (34)$$

By replacing relations (31)-(39) in equation (30), kinetic energy is expressed as:

$$\begin{aligned} \delta T = - \int_0^l \left([b(I_0^t \ddot{u}_0^t + I_1^t \ddot{\phi}^t) \delta u_0^t + b(I_1^t \ddot{u}_0^t \right. \\ \left. + I_2^t \ddot{\phi}^t) \delta \phi^t + bI_0^t \ddot{w}_0^t \delta w_0^t] + [b(I_0^b \ddot{u}_0^b + I_1^b \ddot{\phi}^b) \delta u_0^b \right. \\ \left. + b(I_1^b \ddot{u}_0^b + I_2^b \ddot{\phi}^b) \delta \phi^b + bI_0^b \ddot{w}_0^b \delta w_0^b] \right) dx \\ + \int_{v_c} \rho_c \ddot{u}_c \delta u_c dv - \int_{v_c} \rho_c \ddot{w}_c \delta w_c dv \end{aligned} \quad (35)$$

In the equation (35) the values of I_0^i , I_1^i , and I_2^i are obtained for different distributions of carbon nanotubes as below:

$$I_0^i = \int_{v_i} \rho_i dz \quad (i = t, b) \quad (36)$$

$$I_1^i = \int_{v_i} \rho_i z dz \quad (i = t, b) \quad (37)$$

$$I_2^i = \int_{v_i} \rho_i z^2 dz \quad (i = t, b) \quad (38)$$

After obtaining the strain energy and kinetic energy in the equation (28), the equations of motion are obtained as follows:

$$-b(I_0^t \ddot{u}_0^t + I_1^t \ddot{\phi}^t) + N_{xx,x}^t - \frac{2}{c^2} P_{xx,x}^c + \frac{4}{c^3} Q_{xx,x}^c \quad (39)$$

$$- \frac{2}{c^2} P_{xz,z}^c + \frac{4}{c^3} Q_{xz,z}^c - N_{xz}^c = 0$$

$$\begin{aligned} b(I_1^t \ddot{u}_0^t + I_2^t \ddot{\phi}^t) + M_{xx,x}^t - Q_{xx}^t - \frac{h_t}{c^2} P_{xx,x}^c \\ + \frac{2h_t}{c^3} Q_{xx,x}^c - \frac{h_t}{c^2} P_{xz,z}^c + \frac{2h_t}{c^3} Q_{xz,z}^c - \frac{h_t}{2} N_{xz}^c = 0 \end{aligned} \quad (40)$$

$$-bI_0^t \ddot{u}_0^t + Q_{xx,x}^t + \frac{1}{c} M_{zz,z}^c - \frac{2}{c^2} P_{zz,z}^c + \frac{1}{c} M_{xz,x}^c \quad (41)$$

$$- \frac{2}{c^2} P_{xz,x}^c - N_{zz}^c = 0$$

$$-b(I_0^b \ddot{u}_0^b + I_1^b \ddot{\phi}^b) - N_{xx,x}^b - \frac{2}{c^2} P_{xx,x}^c - \frac{4}{c^3} Q_{xx,x}^c \quad (42)$$

$$- \frac{2}{c^2} P_{xz,z}^c - \frac{4}{c^3} Q_{xz,z}^c + N_{xz}^c = 0$$

$$-b(I_1^b \ddot{u}_0^b + I_2^b \ddot{\phi}^b) + M_{xx,x}^b - Q_{xx}^b + \frac{h_b}{c^2} P_{xx,x}^c \quad (43)$$

$$+ \frac{2h_b}{c^3} Q_{xx,x}^c + \frac{h_b}{c^2} P_{xz,z}^c + \frac{2h_b}{c^3} Q_{xz,z}^c - \frac{h_b}{2} N_{xz}^c = 0$$

$$-bI_0^b \ddot{w}_0^b + Q_{xx,x}^b - \frac{1}{c} M_{zz,z}^c - \frac{2}{c^2} P_{zz,z}^c - \frac{1}{c} M_{xz,x}^c \quad (44)$$

$$- \frac{2}{c^2} P_{xz,x}^c + N_{zz}^c = 0$$

$$-c\rho_c \ddot{u}_c - N_{xx,x}^c + \frac{4}{c^2} P_{xx,x}^c - N_{xz,z}^c \quad (45)$$

$$+ \frac{4}{c^2} P_{xz,z}^c = 0$$

$$-M_{xx,x}^c + \frac{4}{c^2} Q_{xx,x}^c - M_{xz,z}^c + \frac{4}{c^2} Q_{xz,z}^c = 0 \quad (46)$$

$$- \frac{2c}{3} \rho_c \ddot{w}_c - N_{zz,z}^c + \frac{4}{c^2} P_{zz,z}^c - N_{xz,x}^c \quad (47)$$

$$+ \frac{4}{c^2} P_{xz,x}^c = 0$$

In the equations of motion, Equations (39) through (47), the parameters used are defined as:

$$N_{ij}^c = \int_{-c/2}^{c/2} b\sigma_{ij}^c dz \quad (i, j = x, z) \quad (48)$$

$$N_{ij,z}^c = \int_{-c/2}^{c/2} b\sigma_{ij,z}^c dz \quad (i, j = x, z) \quad (49)$$

$$M_{ij}^c = \int_{-c/2}^{c/2} bz\sigma_{ij}^c dz \quad (i, j = x, z) \quad (50)$$

$$M_{ij,z}^c = \int_{-c/2}^{c/2} bz\sigma_{ij,z}^c dz \quad (i, j = x, z) \quad (51)$$

$$P_{ij}^c = \int_{-c/2}^{c/2} bz^2\sigma_{ij}^c dz \quad (i, j = x, z) \quad (52)$$

$$P_{ij,z}^c = \int_{-c/2}^{c/2} bz^2\sigma_{ij,z}^c dz \quad (i, j = x, z) \quad (53)$$

$$Q_{ij}^c = \int_{-c/2}^{c/2} bz^3\sigma_{ij}^c dz \quad (i, j = x, z) \quad (54)$$

$$Q_{ij,z}^c = \int_{-c/2}^{c/2} bz^3\sigma_{ij,z}^c dz \quad (i, j = x, z) \quad (55)$$

$$N_{xx}^i = \int_{-\frac{h_i}{2}}^{\frac{h_i}{2}} b[\sigma_{xx}^i] dz = \int_{-\frac{h_i}{2}}^{\frac{h_i}{2}} b[E_{11}^i \epsilon_{xx}^i] dz \quad (56)$$

$$= \int_{-\frac{h_i}{2}}^{\frac{h_i}{2}} bE_{11}^i \left[\frac{\partial u_0^i}{\partial x} + z \frac{\partial \phi^i}{\partial x} \right] dz \quad (i = t, b)$$

$$N_{xx}^i = A_i \frac{\partial u_0^i}{\partial x} + B_i \frac{\partial \phi^i}{\partial x} \quad (i = t, b) \quad (57)$$

$$M_{xx}^i = \int_{-\frac{h_i}{2}}^{\frac{h_i}{2}} bz[\sigma_{xx}^i] dz = \int_{-\frac{h_i}{2}}^{\frac{h_i}{2}} bz[E_{11}^i \epsilon_{xx}^i] dz \quad (58)$$

$$= \int_{-\frac{h_i}{2}}^{\frac{h_i}{2}} bzE_{11}^i \left[\frac{\partial u_0^i}{\partial x} + z \frac{\partial \phi^i}{\partial x} \right] dz \quad (i = t, b)$$

$$M_{xx}^i = B_i \frac{\partial u_0^i}{\partial x} + C_i \frac{\partial \phi^i}{\partial x} \quad (i = t, b) \quad (59)$$

$$Q_{xx}^i = \int_{-\frac{h_i}{2}}^{\frac{h_i}{2}} bk_s[\tau_{xz}^i] dz = \int_{-\frac{h_i}{2}}^{\frac{h_i}{2}} bk_s[G_{12}^i \gamma_{xz}^i] dz$$

$$= \int_{-\frac{h_i}{2}}^{\frac{h_i}{2}} bk_s G_{12}^i \left[\phi^i + \frac{\partial w_0^i}{\partial x} \right] dz \quad (i = t, b) \quad (60)$$

$$Q_{xx}^i = D_i \left[\phi^i + \frac{\partial w_0^i}{\partial x} \right] \quad (i = t, b) \quad (61)$$

where A_i , B_i , C_i , and D_i are different for different distributions of carbon nanotubes, and these values are obtained according to the following relations:

$$A_i = \int_{-\frac{h_i}{2}}^{\frac{h_i}{2}} bE_{11}^i dz \quad (i = t, b) \quad (62)$$

$$B_i = \int_{-\frac{h_i}{2}}^{\frac{h_i}{2}} bzE_{11}^i dz \quad (i = t, b) \quad (63)$$

$$C_i = \int_{-\frac{h_i}{2}}^{\frac{h_i}{2}} bz^2 E_{11}^i dz \quad (i = t, b) \quad (64)$$

$$D_i = \int_{-\frac{h_i}{2}}^{\frac{h_i}{2}} bk_s G_{12}^i dz \quad (i = t, b) \quad (65)$$

In equations (60) and (65), k_s is the correction coefficient of the shear vector and its value is considered as $k_s = \frac{\pi^2}{12}$ [7]. A_i is tensile strength, B_i is coupling strength, C_i is bending strength, D_i is shear strength for face sheets. Finally, using the relations (48) to (65), the governing equations of motion are expressed as fol-

lows:

$$\begin{aligned} & b(I_1^t \ddot{\phi}_0^t + I_0^t \ddot{u}_0^t) + b \left(\frac{\rho_c c \ddot{u}_0^b}{70} + \frac{\rho_c c \ddot{u}_0^c}{15} + \frac{3\rho_c c \ddot{u}_0^t}{35} - \frac{\rho_c c \ddot{u}_1^c}{70} \right. \\ & - \frac{\rho_c c h_b \ddot{\phi}_0^b}{140} + \frac{3\rho_c c h_t \ddot{\phi}_0^t}{70} \left. \right) + \frac{47bC_{55}^c u_0^t}{15c} - \frac{7bC_{55}^c u_0^b}{15c} \\ & - \frac{8bC_{55}^c u_0^c}{3c} - \frac{\partial^2 u_0^t}{\partial x^2} \left(A_t + \frac{3bcC_{11}^c}{35} \right) \\ & - \frac{bcC_{11}^c}{70} \frac{\partial^2 u_0^b}{\partial x^2} - \frac{bcC_{11}^c}{15} \frac{\partial^2 u_0^c}{\partial x^2} + \frac{4bC_{55}^c u_1^c}{5} \\ & - \frac{\partial^2 \phi_0^t}{\partial x^2} \left(B_t + \frac{3bcC_{11}^c h_t}{70} \right) + \frac{bc^2 C_{11}^c}{70} \frac{\partial^2 u_1^c}{\partial x^2} \\ & + \frac{bcC_{11}^c h_b}{140} \frac{\partial^2 \phi_0^b}{\partial x^2} + \frac{7bC_{55}^c h_b \phi_0^b}{30c} + \frac{47bC_{55}^c h_t \phi_0^t}{30c} \\ & + \frac{\partial w_0^b}{\partial x} \left(\frac{bC_{13}^c}{30} + \frac{bC_{55}^c}{30} \right) - \frac{\partial w_0^c}{\partial x} \left(\frac{2bC_{13}^c}{5} + \frac{2bC_{55}^c}{5} \right) \\ & + \frac{\partial w_0^t}{\partial x} \left(\frac{11bC_{13}^c}{30} - \frac{19bC_{55}^c}{30} \right) = 0 \end{aligned} \quad (66)$$

$$\begin{aligned} & b(I_2^t \ddot{\phi}_0^t + I_1^t \ddot{u}_0^t) + b \left(\frac{3\rho_c c h_t^2 \ddot{\phi}_0^t}{140} - \frac{\rho_c c^2 h_t \ddot{u}_1^c}{140} + \frac{\rho_c c h_t \ddot{u}_0^b}{140} \right. \\ & + \frac{\rho_c c h_t \ddot{u}_0^c}{30} + \frac{3\rho_c c h_t h_t \ddot{u}_0^t}{70} - \frac{\rho_c c h_t h_t \ddot{\phi}_0^b}{280} \left. \right) + \frac{47bC_{55}^c h_t u_0^t}{30c} \\ & - \frac{bcC_{11}^c h_t}{140} \frac{\partial^2 u_0^b}{\partial x^2} - \frac{bcC_{11}^c h_t}{30} \frac{\partial^2 u_0^c}{\partial x^2} - \frac{7bC_{55}^c h_t u_0^b}{30c} - \frac{4bC_{55}^c h_t u_0^c}{3c} \\ & - \frac{\partial^2 u_0^t}{\partial x^2} \left(B_t + \frac{3bcC_{11}^c h_t}{70} \right) + \phi_0^t \left(\frac{47bC_{55}^c h_t^2}{60c} + D_t \right) \\ & - \frac{\partial^2 \phi_0^t}{\partial x^2} \left(\frac{3bcC_{11}^c h_t^2}{140} + C_t \right) + \frac{2bC_{55}^c h_t u_1^c}{5} \\ & + \frac{bc^2 C_{11}^c h_t}{140} \frac{\partial^2 u_1^c}{\partial x^2} + \frac{7bC_{55}^c h_b h_t \phi_0^b}{60c} + \frac{bcC_{11}^c h_b h_t}{280} \frac{\partial^2 \phi_0^b}{\partial x^2} \\ & + \frac{\partial w_0^b}{\partial x} \left(\frac{bC_{13}^c h_t}{60} + \frac{bC_{55}^c h_t}{60} \right) - \frac{\partial w_0^c}{\partial x} \left(\frac{bC_{13}^c h_t}{5} + \frac{bC_{55}^c h_t}{5} \right) \\ & + \frac{\partial w_0^t}{\partial x} \left(D_t + \frac{11bC_{13}^c h_t}{60} - \frac{19bC_{55}^c h_t}{60} \right) = 0 \end{aligned} \quad (67)$$

$$\begin{aligned} & b \left(\frac{\rho_c \ddot{w}_0^c}{15} - \frac{\rho_c c \ddot{w}_0^b}{30} + \frac{2\rho_c c \ddot{w}_0^t}{15} \right) + I_0^t b \ddot{w}_0^t \\ & + \frac{\partial u_0^b}{\partial x} \left(\frac{bC_{13}^c}{30} + \frac{bC_{55}^c}{30} \right) - \frac{\partial u_0^c}{\partial x} \left(\frac{2bC_{13}^c}{3} + \frac{2bC_{55}^c}{3} \right) \\ & - \frac{\partial u_0^t}{\partial x} \left(\frac{11bC_{13}^c}{30} - \frac{19bC_{55}^c}{30} \right) + \frac{\partial u_1^c}{\partial x} \left(\frac{2bcC_{13}^c}{15} + \frac{2bcC_{55}^c}{15} \right) \\ & - \frac{\partial \phi_0^b}{\partial x} \left(\frac{bC_{13}^c h_b}{60} + \frac{bC_{55}^c h_b}{60} \right) - \frac{\partial \phi_0^t}{\partial x} \left(D_t + \frac{11bC_{13}^c h_t}{60} \right) \end{aligned}$$

$$\begin{aligned}
& - \frac{19bC_{55}^c h_t}{60} + \frac{bC_{33}^c w_0^b}{3c} - \frac{\partial^2 w_0^t}{\partial x^2} \left(D_t + \frac{2bcC_{55}^c}{15} \right) + \frac{\partial u_1^c}{\partial x} \left(\frac{2bcC_{13}^c}{15} + \frac{2bcC_{55}^c}{15} \right) - \frac{\partial \phi_0^t}{\partial x} \left(\frac{bC_{13}^c h_t}{60} + \frac{bC_{55}^c h_t}{60} \right) \\
& - \frac{8bC_{33}^c w_0^c}{3c} + \frac{7bC_{33}^c w_0^t}{3c} + \frac{bcC_{55}^c}{30} \frac{\partial^2 w_0^c}{\partial x^2} - \frac{\partial \phi_0^b}{\partial x} \left(D_b + \frac{11bC_{13}^c h_b}{60} - \frac{19bC_{55}^c h_b}{60} \right) + \frac{7bC_{33}^c w_0^b}{3c} \\
& - \frac{bcC_{55}^c}{15} \frac{\partial^2 w_0^c}{\partial x^2} = 0 \quad (68) \quad - \frac{\partial^2 w_0^b}{\partial x^2} \left(D_b + \frac{2bcC_{55}^c}{15} \right) - \frac{8bC_{33}^c w_0^c}{3c} + \frac{bcC_{33}^c w_0^t}{3c}
\end{aligned}$$

$$\begin{aligned}
& b(I_2^b \ddot{\phi}_0 + I_1^b \ddot{u}_0^t) + b \left(\frac{3\rho_c c h_t^2 \ddot{u}_0^b}{35} + \frac{\rho_c c^2 h_t \ddot{u}_1^b}{15} + \frac{\rho_c c \ddot{u}_0^t}{70} \right) - \frac{bcC_{55}^c}{15} \frac{\partial^2 w_0^c}{\partial x^2} + \frac{bcC_{55}^c}{30} \frac{\partial^2 w_0^t}{\partial x^2} = 0 \quad (71) \\
& + \frac{\rho_c c^2 \ddot{u}_1^c}{70} - \frac{3\rho_c c h_b \ddot{\phi}_0^b}{70} + \frac{\rho_c c h_b \ddot{\phi}_0^b}{70} + \frac{\rho_c c h_t \ddot{\phi}_0^t}{140} + \frac{47bC_{55}^c u_0^b}{15c} b \left(\frac{\rho_c c \ddot{u}_0^b}{15} + \frac{8\rho_c c \ddot{u}_0^c}{15} + \frac{\rho_c c \ddot{u}_0^t}{15} - \frac{\rho_c c h_b \ddot{\phi}_0^b}{30} + \frac{\rho_c c h_b \ddot{\phi}_0^t}{30} \right)
\end{aligned}$$

$$\begin{aligned}
& - \frac{\partial^2 u_0^b}{\partial x^2} \left(A_b + \frac{3bcC_{11}^c}{35} \right) - \frac{8bC_{55}^c u_0^c}{3c} - \frac{7bC_{55}^c u_0^t}{15c} + \frac{16bC_{55}^c u_0^c}{3c} - \frac{8bC_{55}^c u_0^b}{3c} - \frac{8bC_{55}^c u_0^t}{3c} - \frac{bcC_{11}^c}{15} \frac{\partial^2 u_0^b}{\partial x^2} \\
& - \frac{bcC_{11}^c}{15} \frac{\partial^2 u_0^c}{\partial x^2} - \frac{bcC_{11}^c}{70} \frac{\partial^2 u_0^t}{\partial x^2} - \frac{\partial^2 \phi_0^b}{\partial x^2} \left(B_b - \frac{3bcC_{11}^c h_b}{70} \right) - \frac{8bcC_{11}^c}{15} \frac{\partial^2 u_0^c}{\partial x^2} - \frac{bcC_{11}^c}{15} \frac{\partial^2 u_0^t}{\partial x^2} + \frac{bcC_{11}^c h_b}{30} \frac{\partial^2 \phi_0^b}{\partial x^2} - \frac{bcC_{11}^c h_t}{30} \frac{\partial^2 \phi_0^t}{\partial x^2} \\
& - \frac{4bC_{55}^c u_1^c}{5} - \frac{bc^2 C_{11}^c}{70} \frac{\partial^2 u_1^c}{\partial x^2} - \frac{bcC_{11}^c h_t}{140} \frac{\partial^2 \phi_0^t}{\partial x^2} - \frac{47bC_{55}^c h_b \phi_0^b}{30c} + \frac{4bC_{55}^c h_b \phi_0^b}{3c} - \frac{4bC_{55}^c h_t \phi_0^t}{3c} + \frac{\partial w_0^t}{\partial x} \left(\frac{2bC_{13}^c}{3} + \frac{2bC_{55}^c}{3} \right) \\
& - \frac{7bC_{55}^c h_t \phi_0^t}{30c} + \frac{\partial w_0^c}{\partial x} \left(\frac{2bC_{13}^c}{5} + \frac{2bC_{55}^c}{5} \right) - \frac{\partial w_0^b}{\partial x} \left(\frac{11bC_{13}^c}{30} - \frac{\partial w_0^b}{\partial x} \left(\frac{2bC_{13}^c}{3} + \frac{2bC_{55}^c}{3} \right) = 0 \quad (72)
\end{aligned}$$

$$\begin{aligned}
& - \frac{19bC_{55}^c}{30} - \frac{\partial w_0^t}{\partial x} \left(\frac{bC_{13}^c}{30} + \frac{bC_{55}^c}{30} \right) = 0 \quad (69) \quad - b \left(\frac{\rho_c c^2 \ddot{u}_0^t}{70} - \frac{\rho_c c^2 \ddot{u}_0^b}{70} - \frac{2\rho_c c^3 \ddot{u}_1^c}{105} + \frac{\rho_c c^2 h_b \ddot{\phi}_0^b}{140} + \frac{\rho_c c^2 h_t \ddot{\phi}_0^t}{140} \right)
\end{aligned}$$

$$\begin{aligned}
& - b \left(\frac{\rho_c c^2 h_b \ddot{u}_1^c}{140} - \frac{3\rho_c c h_b^2 \ddot{\phi}_0^b}{140} + \frac{3\rho_c c h_b \ddot{u}_0^b}{70} + \frac{\rho_c c h_b \ddot{u}_0^c}{30} \right) + \frac{4bC_{55}^c u_0^t}{5} - \frac{4bC_{55}^c u_0^b}{5} - \frac{bc^2 C_{11}^c u_0^b}{70} - \frac{bc^2 C_{11}^c}{70} \frac{\partial^2 u_0^b}{\partial x^2} \\
& + \frac{\rho_c c h_b \ddot{u}_0^t}{140} + \frac{\rho_c c h_b h_t \ddot{\phi}_0^t}{280} + b(I_2^b \ddot{\phi}_0 + I_1^b \ddot{u}_0^b) + \frac{bc^2 C_{11}^c}{70} \frac{\partial^2 u_0^t}{\partial x^2} + \frac{4bcC_{55}^c u_1^c}{5} - \frac{2bc^3 C_{11}^c}{105} \frac{\partial^2 u_1^c}{\partial x^2} + \frac{2bC_{55}^c h_b \phi_0^b}{5} \\
& \frac{bC_{11}^c h_b}{30} \frac{\partial^2 u_0^c}{\partial x^2} - \frac{\partial^2 u_0^b}{\partial x^2} \left(B_b - \frac{3bcC_{11}^c h_b}{70} \right) + \frac{bcC_{11}^c h_b}{140} \frac{\partial^2 u_0^t}{\partial x^2} + \frac{2bC_{55}^c h_t \phi_0^t}{5} + \frac{bc^2 C_{11}^c h_b}{140} \frac{\partial^2 \phi_0^b}{\partial x^2} + \frac{bc^2 C_{11}^c h_t}{140} \frac{\partial^2 \phi_0^t}{\partial x^2}
\end{aligned}$$

$$\begin{aligned}
& - \frac{47bC_{55}^c h_b u_0^b}{30c} + \frac{4bC_{55}^c h_b u_0^c}{3c} + \frac{7bC_{55}^c h_b u_0^t}{30c} + \phi_0^b \left(\frac{47bC_{55}^c h_b^2}{60c} + \frac{\partial w_0^c}{\partial x} \left(\frac{4bcC_{13}^c}{15} + \frac{4bcC_{55}^c}{15} \right) - \frac{\partial w_0^b}{\partial x} \left(\frac{2bcC_{13}^c}{15} + \frac{2bcC_{55}^c}{15} \right) \right) \\
& + D_b) - \frac{\partial^2 \phi_0^b}{\partial x^2} \left(\frac{3bcC_{11}^c h_b^2}{140} + C_b \right) + \frac{2bC_{55}^c h_b u_1^c}{5} - \frac{\partial w_0^t}{\partial x} \left(\frac{2bcC_{13}^c}{15} + \frac{2bcC_{55}^c}{15} \right) = 0 \quad (73)
\end{aligned}$$

$$\begin{aligned}
& + \frac{bc^2 C_{11}^c h_b}{140} \frac{\partial^2 u_1^c}{\partial x^2} + \frac{7bC_{55}^c h_b h_t \phi_0^t}{60c} + \frac{bcC_{11}^c h_b h_t}{280} \frac{\partial^2 \phi_0^t}{\partial x^2} b \left(\frac{\rho_c c \ddot{w}_0^b}{15} + \frac{8\rho_c c \ddot{w}_0^c}{15} + \frac{\rho_c c \ddot{w}_0^t}{15} \right) + \frac{\partial u_0^t}{\partial x} \left(\frac{2bC_{13}^c}{5} \right) \\
& + \frac{\partial w_0^t}{\partial x} \left(\frac{bC_{13}^c h_b}{60} + \frac{bC_{55}^c h_b}{60} \right) - \frac{\partial w_0^c}{\partial x} \left(\frac{bC_{13}^c h_b}{5} + \frac{bC_{55}^c h_b}{5} \right) + \frac{2bC_{55}^c}{5} - \frac{\partial u_0^b}{\partial x} \left(\frac{2bC_{13}^c}{5} + \frac{2bC_{55}^c}{5} \right) + \frac{\partial \phi_0^b}{\partial x} \left(\frac{bC_{13}^c h_b}{5} \right) \\
& + \frac{\partial w_0^b}{\partial x} \left(D_b + \frac{11bC_{13}^c h_b}{60} - \frac{19bC_{55}^c h_b}{60} \right) = 0 \quad (70) \quad + \frac{bC_{55}^c h_b}{5} - \frac{\partial u_1^c}{\partial x} \left(\frac{4bcC_{13}^c}{15} + \frac{4bcC_{55}^c}{15} \right) + \frac{\partial \phi_0^t}{\partial x} \left(\frac{bC_{13}^c h_t}{5} \right)
\end{aligned}$$

$$\begin{aligned}
& b \left(\frac{\rho_c c \ddot{w}_0^b}{15} + \frac{\rho_c c \ddot{w}_0^c}{15} - \frac{\rho_c c \ddot{w}_0^t}{30} \right) + I_0^b b \ddot{w}_0^b + \frac{\partial u_0^b}{\partial x} \left(\frac{11bC_{13}^c}{30} + \frac{bC_{55}^c h_t}{5} \right) + \frac{16bC_{33}^c w_0^c}{3c} - \frac{8bC_{33}^c w_0^b}{3c} - \frac{8bC_{33}^c w_0^t}{3c} \\
& - \frac{19bC_{55}^c}{30} + \frac{\partial u_0^c}{\partial x} \left(\frac{2bC_{13}^c}{3} + \frac{2bC_{55}^c}{3} \right) - \frac{\partial u_0^t}{\partial x} \left(\frac{bC_{13}^c}{30} + \frac{bC_{55}^c}{30} \right) - \frac{bcC_{55}^c}{15} \frac{\partial^2 w_0^b}{\partial x^2} - \frac{8bcC_{55}^c}{15} \frac{\partial^2 w_0^c}{\partial x^2} - \frac{bcC_{55}^c}{15} \frac{\partial^2 w_0^t}{\partial x^2} = 0 \quad (74)
\end{aligned}$$

In this research, the Navier method is used to solve the motion equations and for achieving the natural frequency of sandwich beam with the face sheets of carbon nanotubes. Using nine equations of motions, mass gravity matrices and stiffness matrices will be obtained as follows:

$$M\ddot{y} + Ky = f \quad (75)$$

$$f^T = [0 \ 0 \ 0 \ 0 \ 0 \ 0 \ 0 \ 0 \ 0] \quad (76)$$

$$y^T = [u_0^t \ \phi_0^t \ w_0^t \ u_0^b \ \phi_0^b \ w_0^b \ u_0^c \ u_1^c \ w_0^c] \quad (77)$$

For the simply supported beam, the following relations are considered, and mass and stiffness matrices are calculated.

$$u_0^i(x, t) = U_0^i \cos(\alpha x) e^{i\omega t} \quad (i = t, b, c) \quad (78)$$

$$u_1^c(x, t) = U_1^c \cos(\alpha x) e^{i\omega t} \quad (79)$$

$$\phi_0^i(x, t) = \phi_0^i \cos(\alpha x) e^{i\omega t} \quad (i = t, b) \quad (80)$$

$$w_0^i(x, t) = W_0^i \sin(\alpha x) e^{i\omega t} \quad (i = t, b, c) \quad (81)$$

$$\alpha = n\pi/L \quad (82)$$

By replacing the relations (78), (79), (80), and (81) in the equation (75), the following relation is obtained.

$$(-w^2 \bar{M} + \bar{K}) \bar{y} = 0 \quad (83)$$

$$\bar{y} = [U_0^t \ \phi_0^t \ W_0^t \ U_0^b \ \phi_0^b \ W_0^b \ U_0^c \ U_1^c \ W_0^c] \quad (84)$$

7. Results and Discussion

First of all, the results are verified to ensure the present formulation. For this purpose, the results of this study are compared with those obtained by Wu et al. [7]. The geometric and mechanical properties of the beam are as follows:

Elasticity modulus of matrix is $E_m = 2.5\text{GPa}$ and density of matrix is $\rho_m = 1190\text{kg/m}^3$. density of nanotubes is $m = 0.3$ and $E_{11}^{cn} = 5.6466\text{TPa}$, $G_{12}^{cn} = 1.9445\text{TPa}$, $\rho_{cn} = 1400\text{kg/m}^3$ and $c_n = 0.175$. All of these values are at room temperature and for the hard core $E_c = 113.8\text{GPa}$, $\rho_c = 4430\text{kg/m}^3$, $c = 0.342$ as well as for flexible core values are $E_c = 6.89\text{MPa}$, $\rho_c = 97\text{kg/m}^3$ and $c = 0.342$, The scale-dependent parameters for carbon nanotubes are as follows: for $v_{cn}^* = 0.12$, $\eta_1 = 0.137$ and $\eta_3 = 0.715$ for $v_{cn}^* = 0.17$, $\eta_1 = 0.142$ and $\eta_3 = 1.138$ and for a volume fraction $v_c n^* = 0.28$ $\eta_1 = 0.141$ and $\eta_3 = 1.109$.

The characteristics of the sandwich beam are assumed to be $L = 200\text{mm}$, $b = 10\text{mm}$, $c = 8\text{mm}$ and $h_t = h_b = 1\text{mm}$. It is assumed that L is the length of the beam and c is the thickness of the core and b is the width of the beam. Results are made dimensionless in terms of relation $wL\sqrt{(\rho_c(1-v_c^2)/E_c)}$. The results for the first three natural frequencies are calculated and reported in tables (2) and (3). Tables (2) and (3) show that there is a good matching between the obtained results and the results of Wu et al. Of course the results are a little less in magnitude from the results of Wu et al. The reason is that in the research done by Wu et al. the Timoshenko's theory was used for modeling the entire beam that led to errors while this research is developed based on the sandwich high order theory.

Table 2

Non-dimensional natural frequency of sandwich beam with stiff core and carbon nanotube sheets with UD distribution and $v_{cn}^* = 0.12$.

| | First mode | Second mode | Third mode |
|---------------------|------------|-------------|------------|
| Current article [7] | 0.1401 | 0.5510 | 1.2075 |
| | 0.1432 | 0.5650 | 1.2429 |

Table 3

Non-dimensional natural frequency of sandwich beam with stiff core and carbon nanotube sheets with FG-V distribution and $v_{cn}^* = 0.12$.

| | First mode | Second mode | Third mode |
|---------------------|------------|-------------|------------|
| Current article [7] | 0.1421 | 0.5565 | 1.2122 |
| | 0.1453 | 0.5730 | 1.2599 |

After validation of the results, the effect of different factors such as carbon nanotubes volume fraction, carbon nanotubes distribution in sheets, and geometry on natural frequency is investigated. For this purpose, the characteristics of the sandwich beam in this research are $L = 125\text{mm}$, $b = 30\text{mm}$ and $c = 8\text{mm}$. In Tables 4-8, the effect of the ratio of the thickness of the core to the face sheet thickness $\left(\frac{c}{h_t}\right)$ is studied. The first four natural frequencies are obtained for different distributions of carbon nanotubes. In these tables, carbon nanotubes volume fraction is considered equal to 0.12 with a stiff core.

Table 4

Natural frequency (Hz) for UD distribution in terms of $\left(\frac{c}{h_t}\right)$.

| $\left(\frac{c}{h_t}\right)$ | First mode | Second mode | Third mode | Fourth mode |
|------------------------------|------------|-------------|------------|-------------|
| 4 | 1824.02 | 6598.59 | 13277.32 | 21277.43 |
| 6 | 1613.47 | 6092.34 | 12696.08 | 20780.68 |
| 8 | 1502.77 | 5767.55 | 12229.16 | 20291.96 |

Table 5

Natural frequency (Hz) for FG-O distribution in terms of $\left(\frac{c}{h_t}\right)$.

| $\left(\frac{c}{h_t}\right)$ | First mode | Second mode | Third mode | Fourth mode |
|------------------------------|------------|-------------|------------|-------------|
| 4 | 1822.97 | 6600.40 | 13246.07 | 21133.48 |
| 6 | 1612.81 | 6093.58 | 12694.06 | 20747.37 |
| 8 | 1502.39 | 5767.97 | 12230.53 | 20285.16 |

It can be seen from Tables 4 through 8 that, regardless of the distribution of carbon nanotubes, as the thickness of the face sheets increases, the natural frequency of the system also increases. The reason is that as the thickness of the faces increases, the total stiffness of the structures increases. Moreover, according to these tables, it can be observed that the FG-V distribution of the carbon nanotubes leads to the highest natural frequency and the FG-A distribution leads to the lowest natural frequency. In Figs. 3 to 7, the modal displacement, w_t , for different distributions of carbon nanotubes is drawn.

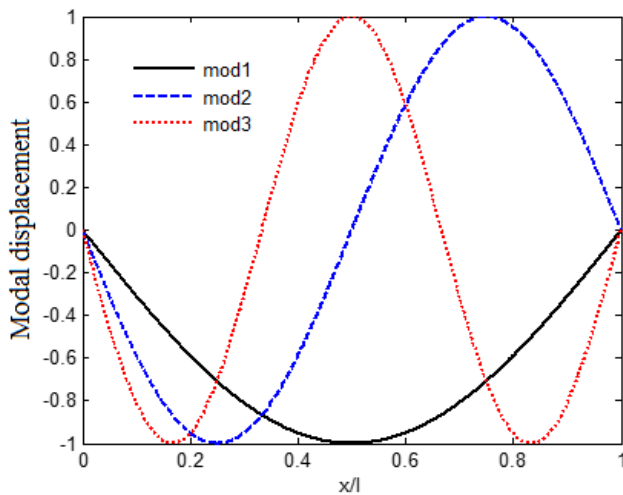


Fig. 3. w_t vibrational mod for UD distribution.

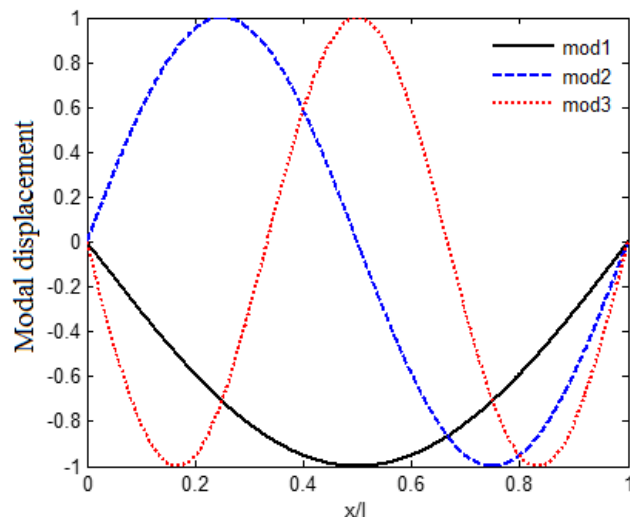


Fig. 4. w_t vibrational mod for FG-O distribution.

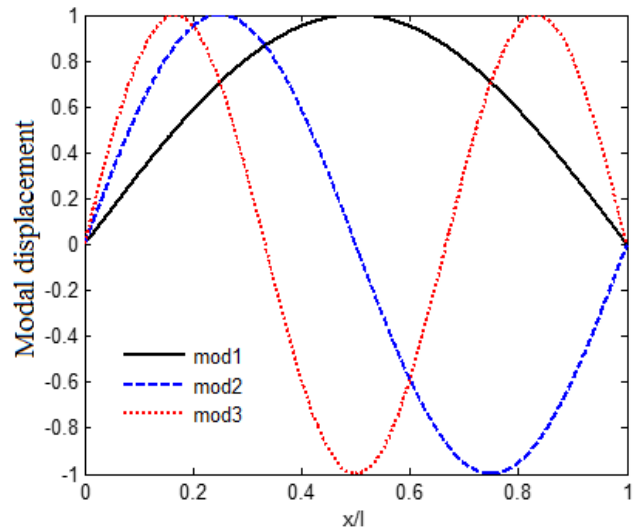


Fig. 5. w_t vibrational mod for FG-X distribution.

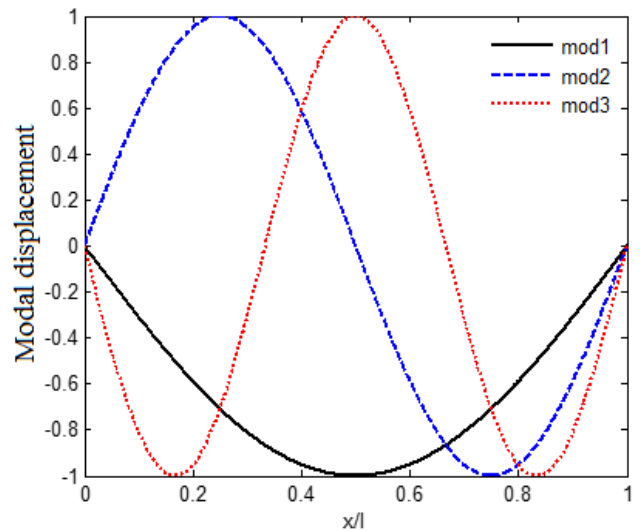


Fig. 6. w_t vibrational mod for FG-V distribution.

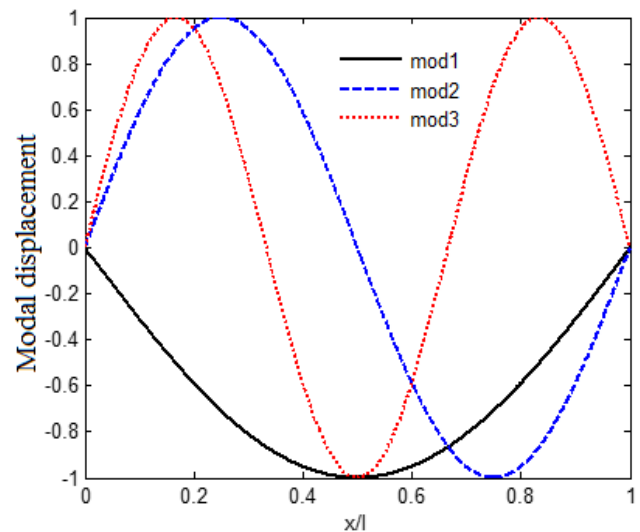


Fig. 7. w_t vibrational mod for FG-A distribution.

Table 6

Natural frequency (Hz) for FG-X distribution in terms of $\left(\frac{c}{h_t}\right)$.

| $\left(\frac{c}{h_t}\right)$ | First mode | Second mode | Third mode | Fourth mode |
|------------------------------|------------|-------------|------------|-------------|
| 4 | 1825.69 | 6602.65 | 13318.70 | 21418.95 |
| 6 | 1614.33 | 6093.63 | 12705.77 | 20824.84 |
| 8 | 1503.24 | 5768.38 | 12232.31 | 20307.67 |

Table 7

Natural frequency (Hz) for FG-V distribution in terms of $\left(\frac{c}{h_t}\right)$.

| $\left(\frac{c}{h_t}\right)$ | First mode | Second mode | Third mode | Fourth mode |
|------------------------------|------------|-------------|------------|-------------|
| 4 | 1861.44 | 6510.32 | 12820.12 | 20345.52 |
| 6 | 1639.40 | 6085.89 | 12489.50 | 20242.42 |
| 8 | 1520.59 | 5782.53 | 12139.05 | 19983.42 |

In Tables 9 to 13, the effect of the volume fraction of carbon nanotubes on the first four natural frequencies for the simply supported boundary conditions and the various distributions of carbon nanotubes is expressed. In these tables, the ratio of core thickness to the face sheet thickness is $\frac{c}{h_t} = 4$, and the results are expressed for three volumes of carbon nanotubes.

Table 8

Natural frequency (Hz) for FG- Λ distribution in terms of $\left(\frac{c}{h_t}\right)$.

| $\left(\frac{c}{h_t}\right)$ | First mode | Second mode | Third mode | Fourth mode |
|------------------------------|------------|-------------|------------|-------------|
| 4 | 1774.63 | 6627.30 | 13649.64 | 22118.89 |
| 6 | 1583.24 | 6064.80 | 12825.24 | 21216.17 |
| 8 | 1483.02 | 5733.83 | 12264.48 | 20508.44 |

Table 9

Natural frequency (Hz) for UD distribution in terms of v_{cn}^* .

| v_{cn}^* | First mode | Second mode | Third mode | Fourth mode |
|------------|------------|-------------|------------|-------------|
| 0.12 | 1824.02 | 6598.59 | 13277.32 | 21277.43 |
| 0.17 | 2077.95 | 7465.89 | 14843.34 | 23464.26 |
| 0.28 | 2456.94 | 8489.18 | 16379.37 | 25414.01 |

Table 10

Natural frequency (Hz) for FG-O distribution in terms of v_{cn}^* .

| v_{cn}^* | First mode | Second mode | Third mode | Fourth mode |
|------------|------------|-------------|------------|-------------|
| 0.12 | 1822.97 | 6600.40 | 13246.07 | 21133.48 |
| 0.17 | 2076.64 | 7473.65 | 14832.59 | 23349.63 |
| 0.28 | 2460.65 | 8531.55 | 16404.86 | 25274.91 |

Table 11

Natural frequency (Hz) for FG-X distribution in terms of v_{cn}^* .

| v_{cn}^* | First mode | Second mode | Third mode | Fourth mode |
|------------|------------|-------------|------------|-------------|
| 0.12 | 1825.69 | 6602.65 | 13318.70 | 21418.95 |
| 0.17 | 2080.89 | 7474.18 | 14893.01 | 23624.53 |
| 0.28 | 2464.43 | 8539.92 | 16561.96 | 25824.23 |

Table 12

Natural frequency (Hz) for FG-V distribution in terms of v_{cn}^* .

| v_{cn}^* | First mode | Second mode | Third mode | Fourth mode |
|------------|------------|-------------|------------|-------------|
| 0.12 | 1861.44 | 6510.32 | 12820.12 | 20345.52 |
| 0.17 | 2133.02 | 7400.98 | 14348.02 | 22381.01 |
| 0.28 | 2516.87 | 8334.61 | 15644.06 | 23940.54 |

Table 13

Natural frequency (Hz) for FG- Λ distribution in terms of v_{cn}^* .

| v_{cn}^* | First mode | Second mode | Third mode | Fourth mode |
|------------|------------|-------------|------------|-------------|
| 0.12 | 1774.63 | 6627.30 | 13649.64 | 22118.89 |
| 0.17 | 2009.14 | 7460.56 | 15230.91 | 24426.75 |
| 0.28 | 2383.95 | 8623.74 | 17149.25 | 26939.59 |

As can be seen in Tables 9 through 13, regardless of distributions of carbon nanotubes, the natural frequency increases by increasing the volume fraction of carbon nanotubes. This is because the elasticity modulus of the carbon nanotubes is larger than the rest of the components, therefore increasing the volume fraction of the carbon nanotubes increases the stiffness of the whole beam. Therefore, the natural frequency of the system increases. From the results of Table 9-13, it is evident that, regardless of the variation of the carbon volume fraction, the maximum natural frequency of the first mode is related to the FG-V distribution mode and the lowest natural frequency of the first mode is related to the FG- Λ distribution state. Considering the use of a stiff core in this paper, the results are for a state in which the axial stresses of the core is considered along the length of the beam. In Table 14 for the distribution of FG-X carbon nanotubes, $v_{cn}^* = 0.12$ and $\frac{c}{h_t} = 4$, shows the effect of axial stresses of the core on the first four natural frequencies.

Table 14

Natural frequency (Hz) for considering and not considering the axial stresses of the core along the length of the beam.

| | First mode | Second mode | Third mode | Fourth mode |
|------------------------|------------|-------------|------------|-------------|
| $\sigma_{xx}^c \neq 0$ | 1825.69 | 6602.65 | 13318.70 | 21418.95 |
| $\sigma_{xx}^c = 0$ | 1471.02 | 5156.13 | 10044.06 | 15704.50 |

It is clear from Table 13 that the difference in the first vibrational mode is 19.42%, which is due to the fact that the normal stress of the core is not considered along the length of the beam. Therefore, due to this great difference, which occurred for the stiff cores, it can be concluded that the axial stresses of the core (which is ignored in many researches) must be considered for robust analyses.

In this section, the analysis of free vibration of sandwich beam with the face sheets with carbon nanotubes and flexible core is studied. For this purpose, the values for the core are considered $E_c = 6.89\text{MPa}$, $\rho_c = 97\text{kg/m}^3$ and $\nu_c = 0.342$. In Tables 15 to 19, the

effect of the ratio of the thickness of the core to the face sheet thickness of the first four natural frequencies for the simply supported boundary conditions and the various distributions of carbon nanotubes is expressed. In these tables, the carbon volume fraction is considered to be $v_{cn}^* = 0.12$.

Table 15

Natural frequency (Hz) for UD distribution in terms of $\left(\frac{c}{h_t}\right)$.

| $\left(\frac{c}{h_t}\right)$ | First mode | Second mode | Third mode | Fourth mode |
|------------------------------|------------|-------------|------------|-------------|
| 4 | 556.53 | 1891.32 | 3880.61 | 6290.15 |
| 6 | 450.70 | 1367.32 | 2786.24 | 4621.36 |
| 8 | 421.37 | 1134.96 | 2219.52 | 3654.57 |

Table 16

Natural frequency (Hz) for FG-O distribution in terms of $\left(\frac{c}{h_t}\right)$.

| $\left(\frac{c}{h_t}\right)$ | First mode | Second mode | Third mode | Fourth mode |
|------------------------------|------------|-------------|------------|-------------|
| 4 | 452.43 | 1451.82 | 3003.58 | 4996.61 |
| 6 | 397.85 | 1093.04 | 2161.92 | 3585.13 |
| 8 | 391.96 | 958.28 | 1777.35 | 2865.16 |

Table 17

Natural frequency (Hz) for FG-X distribution in terms of $\left(\frac{c}{h_t}\right)$.

| $\left(\frac{c}{h_t}\right)$ | First mode | Second mode | Third mode | Fourth mode |
|------------------------------|------------|-------------|------------|-------------|
| 4 | 641.74 | 2213.56 | 4466.77 | 7078.31 |
| 6 | 497.39 | 1584.76 | 3246.18 | 5334.54 |
| 8 | 448.67 | 1283.54 | 2565.95 | 4237.92 |

Table 18

Natural frequency (Hz) for FG-V distribution in terms of $\left(\frac{c}{h_t}\right)$.

| $\left(\frac{c}{h_t}\right)$ | First mode | Second mode | Third mode | Fourth mode |
|------------------------------|------------|-------------|------------|-------------|
| 4 | 503.70 | 1639.08 | 3375.32 | 5556.00 |
| 6 | 429.45 | 1214.90 | 2426.04 | 4022.04 |
| 8 | 413.99 | 1042.32 | 1968.31 | 3197.79 |

Table 19

Natural frequency (Hz) for FG-A distribution in terms of $\left(\frac{c}{h_t}\right)$.

| $\left(\frac{c}{h_t}\right)$ | First mode | Second mode | Third mode | Fourth mode |
|------------------------------|------------|-------------|------------|-------------|
| 4 | 480.44 | 1612.71 | 3349.44 | 5531.25 |
| 6 | 405.22 | 1181.93 | 2390.77 | 3986.48 |
| 8 | 391.18 | 1006.75 | 1927.22 | 3154.46 |

It can be seen from Tables 15 through 19 that, regardless of the distribution of carbon nanotubes, as the thickness of the face sheets increases, the natural frequency of the system increases too. Additionally, according to the results in Tables 15 to 19, it can be seen that the maximum natural frequency is related

to the FG-X distribution mode and the lowest natural frequency corresponds to the FG-O distribution mode.

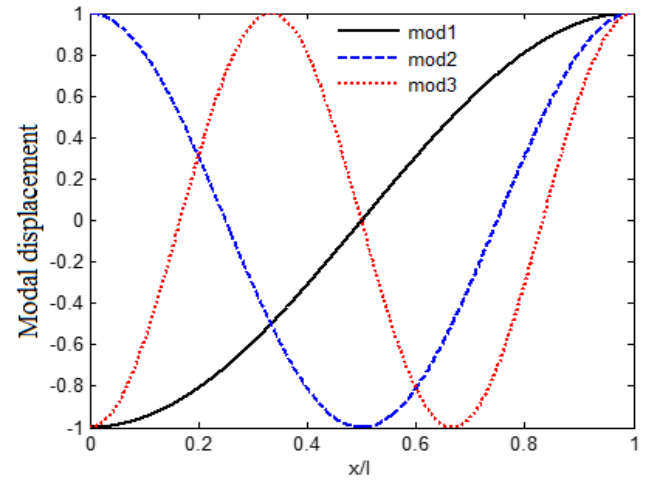


Fig. 8. U_t vibrational mod for UD distribution.

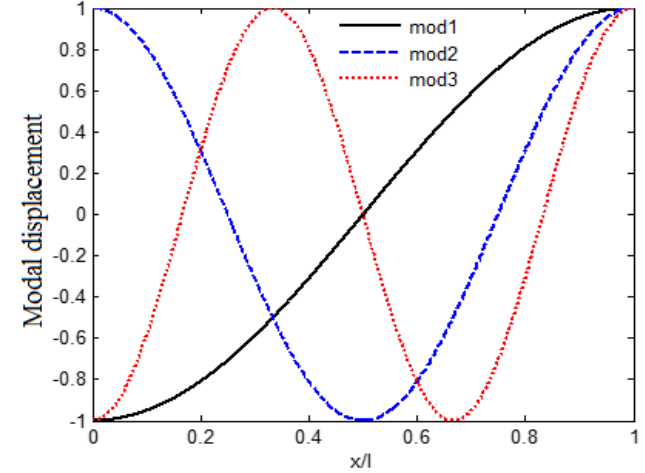


Fig. 9. U_t vibrational mod for FG-O distribution.

In Figs. 8 to 12, the modal displacement of the vibrational mode, U_t , is drawn for the upper face sheets of the various distributions of the carbon nanotubes for the case $v_{cn}^* = 0.12$ and $\frac{c}{h_t} = 4$.

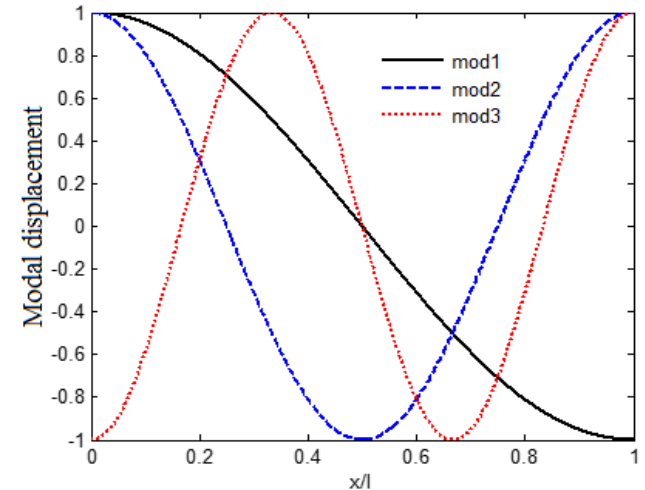


Fig. 10. U_t vibrational mod for FG-X distribution.

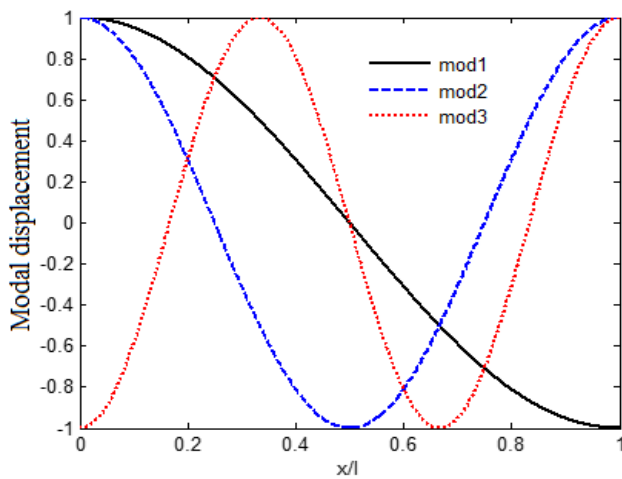


Fig. 11. U_t vibrational mod for FG-V distribution.

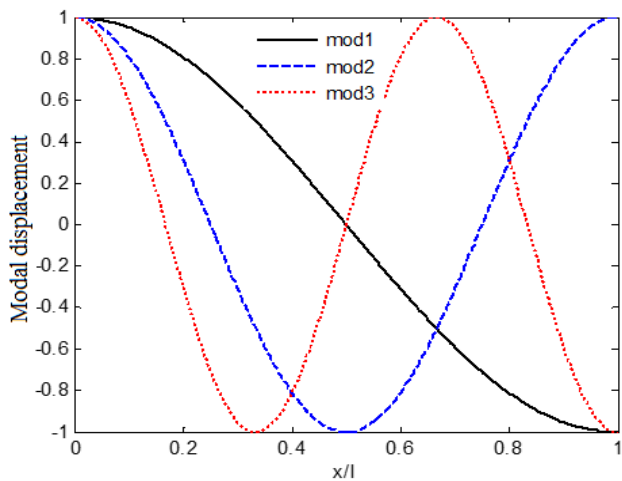


Fig. 12. U_t vibrational mod for FG-A distribution.

In Tables 20 to 24, the effect of the carbon nanotubes on four natural frequencies for simply supported boundary conditions and different distributions of carbon nanotubes is expressed. In these tables, the ratio of the thickness of the core to the face sheet thickness is $\frac{c}{h_t} = 4$, and the results for three volume fractions of carbon nanotubes is expressed.

Table 20
Natural frequency (Hz) for UD distribution in terms of v_{cn}^* .

| v_{cn}^* | First mode | Second mode | Third mode | Fourth mode |
|------------|------------|-------------|------------|-------------|
| 0.12 | 556.53 | 1891.32 | 3880.61 | 6290.15 |
| 0.17 | 639.40 | 2254.89 | 4691.68 | 7660.87 |
| 0.28 | 769.69 | 2754.30 | 5643.38 | 9001.91 |

Table 21
Natural frequency (Hz) for FG-O distribution in terms of v_{cn}^* .

| v_{cn}^* | First mode | Second mode | Third mode | Fourth mode |
|------------|------------|-------------|------------|-------------|
| 0.12 | 452.43 | 1451.82 | 3003.58 | 4996.61 |
| 0.17 | 504.43 | 1699.84 | 3578.74 | 6009.31 |
| 0.28 | 590.32 | 2071.62 | 4364.43 | 7251.34 |

Table 22
Natural frequency (Hz) for FG-X distribution in terms of v_{cn}^* .

| v_{cn}^* | First mode | Second mode | Third mode | Fourth mode |
|------------|------------|-------------|------------|-------------|
| 0.12 | 641.74 | 2213.56 | 4466.77 | 7078.31 |
| 0.17 | 748.06 | 2663.04 | 5447.36 | 8687.46 |
| 0.28 | 911.05 | 3252.44 | 6517.42 | 10119.12 |

Table 23
Natural frequency (Hz) for FG-V distribution in terms of v_{cn}^* .

| v_{cn}^* | First mode | Second mode | Third mode | Fourth mode |
|------------|------------|-------------|------------|-------------|
| 0.12 | 503.70 | 1639.08 | 3375.32 | 5556.00 |
| 0.17 | 565.82 | 1928.39 | 4038.90 | 6709.97 |
| 0.28 | 666.82 | 2350.54 | 4904.12 | 8030.19 |

As shown in Tables 20 to 24, regardless of the different distributions of carbon nanotubes, the natural frequency increases by increasing the nanotubes volume fraction. From the review of the results in Tables 20 to 24, it is clear that regardless of the variation of the carbon volume fraction, the highest natural frequency of the first mode is related to the FG-X distribution mode, and the lowest natural frequency of the first modulus is in the distribution of FG-A.

Table 24
Natural frequency (Hz) for FG-A distribution in terms of v_{cn}^* .

| v_{cn}^* | First mode | Second mode | Third mode | Fourth mode |
|------------|------------|-------------|------------|-------------|
| 0.12 | 480.44 | 1612.71 | 3349.44 | 5531.25 |
| 0.17 | 545.05 | 1905.64 | 4016.58 | 6688.28 |
| 0.28 | 649.56 | 2332.61 | 4886.90 | 8013.38 |

8. Conclusions

In this study, the free vibrations of sandwich beams with carbon nanotubes and hard and flexible core were investigated. Timoshenko's theory was used to model the face sheets and the compatibility conditions were applied for continuity of the displacement field between the core and the face sheets. Finally, using the variation of energy, the equations of motion of the system were obtained. In this study, the face sheets were considered as composite reinforced with different distributions of carbon nanotubes. In this research, due to the high order displacement field of the core, the flexibility of the core can be seen in the modeling. Since the term σ_{xx}^c of the core is also considered in the strain energy, a stiff core can be modeled. In many works the σ_{xx}^c is removed from equations, therefore according to the results of sandwich beam with stiff core it can be seen that if the σ_{xx}^c is removed from equations, lots of errors will be observed. Therefore, a proposed theory in this research can easily model a sandwich beam with two types of stiff and flexible cores. Numerical results for different volume fractions of carbon for different distributions were investigated. The effect of the geometry

of the beam, such as core thickness, face sheets thickness, etc. was studied on the natural frequency of the system, which yielded the following results:

- Regarding the study of the effect of the distribution of nanotubes on face sheets, it is clear that the highest natural frequency of the first mode for the stiff core is related to the FG-V distribution and for the flexible core it is related to the FG-X distribution.
- The results show that, the lowest natural frequency of the first mode for the stiff core is related to the FG- Λ distribution and the FG-O distribution for the flexible core.
- Due to the core displacement field, a flexible core can be modeled and this displacement field is used in high order theory.
- High order theory is suitable theory for flexible and stiff core.
- Out of the results, it is clear that high order theory has good accuracy.
- The results show that for stiff cores, disregarding the axial stresses of the core, which is carried out in many studies, leads to large error in the results.
- The results also show that extended higher order theory is a suitable model for analyzing a stiff and flexible core sandwich panel.
- As the numerical results show, the natural frequency of the sandwich beam in all the different distributions of carbon nanotubes decreases with the increase of the core-to-face sheet thickness ratio, which is due to the reduction of the total stiffness of the structures.
- By increasing the nanotubes volume fraction, the natural frequency of the system increases.
- By examining the results, it is clear that the volume fraction of carbon nanotubes has the highest effect and the ratio of the core-to-face sheet thickness ratio has the least effect on the normal frequency of the system.

References

- [1] T.E. Lasy, Y. Hwang, Numerical modeling of impact damaged sandwich composites subjected to compression after impact loading, *Compos. Struct.*, 61(1-2) (2003)115-128.
- [2] K. E. Evans, The design of doubly curved sandwich panels with honeycomb cores, *Compos. Struct.*, 17(2) (1991) 95-111.
- [3] Y. Frostig, M. Baruch, O. Vilnay, I. Sheinman, Behavior of delaminated sandwich beam with transversely flexible core - high order theory, *Compos. Struct.*, 20(1) (1992) 1-16.
- [4] E.T. Thostenson, Z. Ren, T. W. Chou, Advances in the science and technology of carbon nanotubes and their composites, *Compos. Sci. Technol.*, 61(13) (2001) 1899-1912.
- [5] M. Meyyappan, *Carbon Nanotubes Science & Applications*, CRC Press, (2004).
- [6] H.S. Shen, Y. Xiang, Nonlinear bending of nanotube reinforced composite cylindrical panels resting on elastic foundations in thermal environments, *Eng. Struct.*, 80 (2014) 163-172.
- [7] H. Wu, S. Kitipornchai and J. Yang, Free vibration and buckling analysis of sandwich beams with functionally graded carbon nanotube reinforced composite face sheets, *Int. J. Struct. Stabil. Dyn.*, 15 (2015) 1-17.
- [8] R.K. Bhangale, N. Ganesan, Thermoplastic buckling and vibration behavior of a functionally graded sandwich beam with constrained viscoelastic core, *J. Sound. Vib.*, 295(1-2) (2006) 294-316.
- [9] H.S. Shen, Nonlinear bending of functionally graded carbon nanotube reinforced composite plates in thermal environments. *Compos. Struct.*, 91(1) (2009) 9-19.
- [10] H.S. Shen, Z.H. Zhu, Post buckling of sandwich plates with nanotube-reinforced composite face sheets resting on elastic foundations, *Eur. J. Mech. A. Solids.*, 35 (2012) 10-21.
- [11] R. Ansari, E. Hasrati, M. Faghih Shojaei, R. Gholi, A. Shahabadini, Forced vibration analysis of functionally graded carbon nanotube reinforced composite plates using a numerical strategy, *Physica. E.*, 69 (2015) 294-305.
- [12] L.L. Ke, J. Yang, S. Kitipornchai, Nonlinear free vibration of functionally graded carbon nanotube-reinforced composite beams, *Compos. Struct.*, 92(3) (2010) 676-683.
- [13] Y. Frostig, Behavior of delaminated sandwich beam with transversely flexible core-high order theory, *Compos. Struct.*, 20(1) (1992) 0-07.
- [14] J.N. Reddy, *Mechanics of laminated composite plates and shells: Theory and analysis*, NewYork, Oxford University Press Inc, Ed2, (2003).
- [15] H.S. Shen, Postbuckling of nanotube-reinforced composite cylindrical shells in thermal environments, Part I: axially-loaded shells, *Compos. Struct.*, 93(8) (2011) 2096-2108.

- [16] Z.X. Wang, J. Xu, P. Qjao, Nonlinear low velocity impact analysis of temperature dependent nanotube reinforced composite plates. *Compos. Struct.*, 108 (2014) 423-434.